Molecular state in a spin–orbital-angular-momentum coupled Fermi gas

Yiwen Han,[1] Shi-Guo Peng,[2] Ke-Ji Chen,[3] and Wei Yi[1,4,*]

[1]*Chinese Academy of Sciences Key Laboratory of Quantum Information, University of Science and Technology of China, Hefei 230026, China*

[2]*State Key Laboratory of Magnetic Resonance and Atomic and Molecular Physics, Innovation Academy for Precision Measurement Science and Technology, Chinese Academy of Sciences, Wuhan 430071, China*

[3]*Key Laboratory of Optical Field Manipulation of Zhejiang Province and Physics Department of Zhejiang Sci-Tech University, Hangzhou 310018, China*

[4]*Chinese Academy of Sciences Center For Excellence in Quantum Information and Quantum Physics, Hefei 230026, China*

(Received 25 March 2022; accepted 19 September 2022; published 3 October 2022)

We study the two-body bound states in a spin-orbital-angular-momentum (SOAM) coupled quantum gas of fermions within a tightly confined ring geometry in two dimensions. Two different configurations are considered: an attractive *s*-wave interaction exists between two spin species that are SOAM coupled and an atom with SOAM coupled internal spins interacts state selectively with another atom. For both cases, we identify the condition for the emergence of molecular states with finite orbital angular momenta. These molecular states with quantized orbital angular momenta correspond to the SOAM-coupling-induced vortices in the corresponding Fermi superfluid. We propose to detect the molecules through Raman spectroscopy with Laguerre-Gaussian lasers. As the molecular states can form above the superfluid temperature, they offer an experimentally more accessible route toward the study of the underlying pairing mechanism under SOAM coupling.

DOI: 10.1103/PhysRevA.106.043302

I. INTRODUCTION

Synthetic spin-orbit coupling in cold atoms modifies the single-particle dispersion and offers a powerful tool for quantum control [1–3]. In the past decade, such control has enabled the simulation of band topology and led to the prediction of various exotic few- and many-body states [4–9]. Building upon these achievements, the recent experimental realization of spin-orbital-angular-momentum (SOAM) coupling introduces even more opportunities [10–20]. Therein, different ground hyperfine states of an atom are coupled by a pair of copropagating Laguerre-Gaussian beams with distinct orbital angular momentum, giving rise to the experimental observation of spin-dependent vortices in spinor Bose-Einstein condensates under SOAM coupling [10,11]. Further, as a direct consequence of the deformed single-particle dispersion in the discretized angular-momentum space, a unique vortex-forming mechanism exists in the SOAM coupled Fermi superfluids [21,22]. It was proposed very recently that an angular topological superfluid can be induced by SOAM coupling [23] whose topological defect, in the form of giant vortices, has interesting implications for topological quantum computation.

Nevertheless, a fundamental hurdle to the experimental observation of the SOAM-coupling-induced pairing states is the inevitable heating introduced by the Raman process [24], which makes it difficult to cool the system below the superfluid temperature. It is one of the key reasons that, despite a plethora of theoretical study on exotic pairing states in spin-orbit coupled Fermi gases, none have so far been observed in experiments. Instead, it is much easier to generate Fesshbach molecules under spin-orbit coupling, which persist above the critical temperature [25,26]. Similarly, it is reasonable to expect that molecular states in a SOAM coupled Fermi gas should be readily accessible under typical experimental conditions and would provide much desired insight into the pairing mechanism under the SOAM coupling.

In this work, we study in detail the molecular state in a SOAM coupled Fermi gas in two dimensions and show that two-body bound states with a quantized orbital angular momentum can be stabilized, leaving detectable signatures in the Raman spectroscopy. We focus on the case of a tightly confined ring geometry and consider two different scenarios. In the first case, a molecular state is formed through an attractive *s*-wave interaction between two hyperfine spin states that are also coupled through the SOAM coupling. The molecule acquires a finite orbital angular momentum under a sufficiently strong Zeeman field that breaks the time-reversal symmetry. The underlying pairing mechanism is similar to that of the SOAM-coupling-induced vortex state in Refs. [21,22] and is the angular analog of the spin-orbit-coupling-induced Fulde-Ferrell state in Ref. [27]. More specifically, under both the SOAM coupling and the Zeeman field, the time-reversal symmetry is broken, leading to an asymmetric single-particle dispersion in the angular-momentum space with respect to $m = 0$. In the many-body setting, the Fermi surface inherits the asymmetry, and the resulting Cooper pair can acquire a finite angular momentum under appropriate parameters. This gives rise to an exotic vortex state. Since the asymmetry emerges on the single-body level, it should also impact molecular formation in the absence of a Fermi sea, offering

*wyiz@ustc.edu.cn

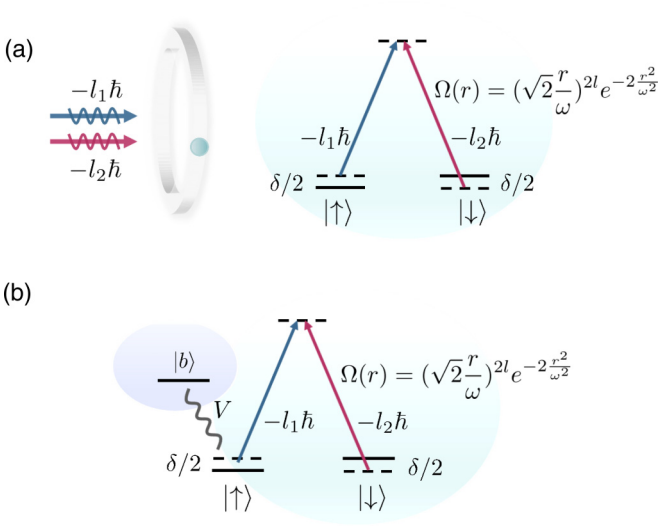

FIG. 1. (a) Schematic illustration of the first scenario, where two spin species with attractive s-wave interaction are Raman coupled by a pair of copropagating Laguerre-Gaussian beams. Due to the spatial light distribution of the lasers, the atoms are effectively trapped in a ring geometry under the scalar Stark potential. (b) Schematic illustration of the second scenario, where the same pair of Laguerre-Gaussian beams couple the internal spin states $|\uparrow\rangle$ and $|\downarrow\rangle$ of the first atom. The other atom (labeled $|b\rangle$) interacts only with the spin-up species. See discussions in the main text for definitions of the various variables.

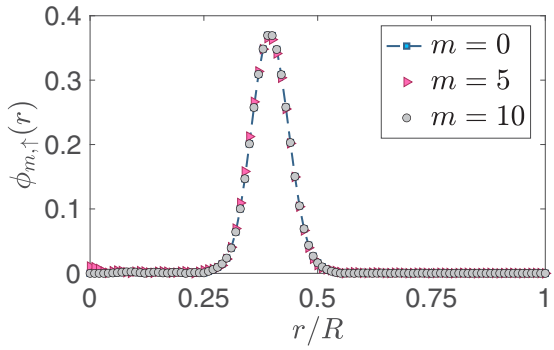

FIG. 2. Radial distribution of the eigen wave function $\phi_{m,\uparrow}(r)$ for different angular-momentum modes. For numerical calculations, we take $l = 5$, $\delta = 0$, $R/w = 4$, and $\chi/E_l = -1$. Here E_l is the unit of energy defined in the main text.

an insightful peek of the exotic pairing mechanism on the two-body level.

In the second case, the SOAM coupling is only enforced upon the internal states of one of the atoms, which interacts with the other atom in a spin-selective fashion. The resulting molecular state also acquires a finite angular momentum due to the interplay between the SOAM coupling and spin-selective interaction [28]. We then propose to detect the molecular state, particularly their quantized angular momentum, through Raman spectroscopy with Laguerre-Gaussian beams. While our calculations are performed within a tightly confined ring geometry, our results are instructive for ring geometries that are less restrictive. Our results suggest that understanding molecules is a natural first step in the experimental study of the unique pairing states under the SOAM coupling.

The paper is organized as follows. In Sec. II, we present the models for the two scenarios. We focus on the characterization of the first scenario in Sec. III, emphasizing the quantized orbital angular momentum of the molecular state and its signal in the direct Raman spectroscopy. In Sec. IV, we focus on the characterization of the second scenario, where we propose a detection scheme based on inverse Raman spectroscopy. We summarize in Sec. V.

II. MODEL

As illustrated in Fig. 1, we consider two different scenarios. In the first scenario [Fig. 1(a)], each of the two atoms is subject to the same SOAM coupling, generated by a pair of Laguerre-Gaussian beams with different orbital angular momentum. While we consider a two-dimensional Fermi gas, the spatial profiles of the overall light field induces a ring-shaped scalar Stark potential within the plane, which restricts the radial atomic motion. An attractive s-wave interaction exists between the two spin species.

In the second scenario [Fig. 1(b)], the SOAM coupling is only applied on the internal spin states of one of the atoms, whereas the other atom (in state $|b\rangle$) interacts only with the spin-up species of the first atom. Thus, the second atom acts as a probe through which information of the SOAM coupling is reflected in the resulting molecular state.

A. Hamiltonian for scenario I

We first write down the single-particle Hamiltonian for the first scenario in the spin basis $\{|\uparrow\rangle, |\downarrow\rangle\}$

$$H_0 = -\frac{\hbar^2\nabla^2}{2M} + V_{\text{ext}}(\mathbf{r}) + \frac{(l\hbar)^2}{2Mr^2} + \chi I(r) + \Omega I(r)\sigma_x + \frac{l\hbar}{Mr^2}L_z\sigma_z + \frac{\delta}{2}\sigma_z, \tag{1}$$

where σ_i $(i = x, y, z)$ are the Pauli matrices, M is the atomic mass, $L_z = -i\hbar\partial/\partial\theta$ is the atomic angular momentum operator in the polar coordinate, $\mathbf{r} = (r, \theta)$, $2l\hbar = (l_2 - l_1)\hbar$ is the transferred orbital angular momentum, and δ is the two-photon detuning of the Raman process generating the SOAM coupling. To derive the Hamiltonian, we have taken a gauge transformation $U = \text{diag}(e^{il\theta}, e^{-il\theta})$, and assumed a hard-wall box potential $V_{\text{ext}}(\mathbf{r})$ with a radius R. Under the spatially inhomogeneous Laguerre-Gaussian beams, the atoms are subject to the Raman and scalar Stark potentials, denoted as $\Omega I(r)$ and $\chi I(r)$, respectively, with $I(r) = (\sqrt{2}r/\omega)^{2l}e^{-2r^2/\omega^2}$. Here w is the laser waist.

Throughout this work, we assume that the scalar Stark potential is sufficiently deep, such that the atomic radial degrees of freedom are frozen into the ground state with $n = 1$. Key features of the molecular state (or pairing states in the many-body case) are preserved in this single-mode approximation [23].

It is then convenient to adopt a second-quantized form of Hamiltonian (1) by expanding the field operators of

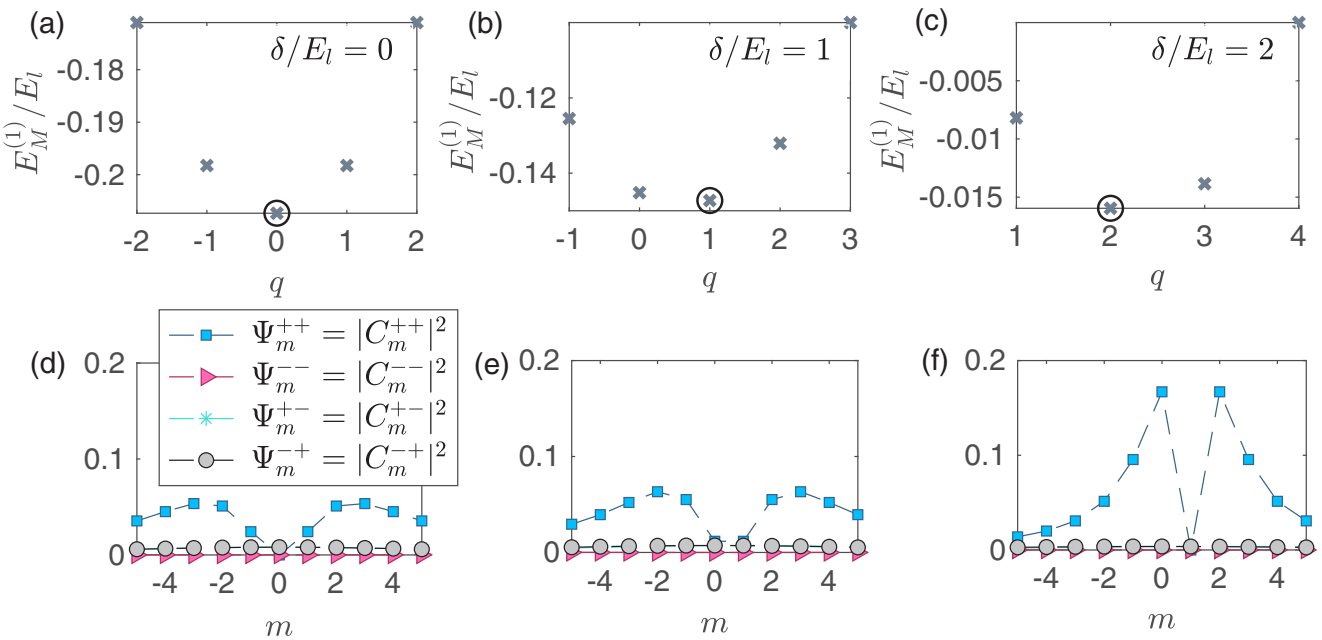

FIG. 3. (a)–(c) The molecular binding energy $E_M^{(1)}$ as functions of the orbital angular momentum q, under different detunings: (a) $\delta = 0$, (b) $\delta/E_l = 1$, (c) $\delta/E_l = 2$. The ground states feature (a) $q = 0$, (b) $q = 1$, (c) $q = 2$. (d)–(f) The ground-state molecular wave function in the discretized angular-momentum space (characterized by m), under the parameters in (a)–(c), respectively. For all calculations, we fix $l = 5$, $E_B^{(1)}/E_l = -6$, $\Omega/E_l = 0.18$.

the two spin species as $\psi_\sigma(\mathbf{r}) = \sum_m \phi_{m,\sigma}(r)\Theta_m(\theta)a_{m,\sigma}$. Here $a_{m,\sigma}$ are the annihilation operators of the corresponding mode, $\Theta_m(\theta) = e^{im\theta}/\sqrt{2\pi}$, and $\phi_{m\sigma}$ are the eigen wave functions of $K_\sigma = -\frac{\hbar^2}{2M}[\frac{1}{r}\frac{\partial}{\partial r}(r\frac{\partial}{\partial r}) + \frac{1}{r^2}(\frac{\partial}{\partial\theta} + i\tau l)^2] + V_{\text{ext}}(r) + \chi I(r) + \tau\frac{\delta}{2}$, with $\tau = +1$ (-1) for $\sigma = \uparrow$ $(\downarrow)$. Specifically, we have

$$K_\sigma(\mathbf{r})\phi_{m,\sigma}(r)\Theta_m(\theta) = \epsilon_{m,\sigma}\phi_{m,\sigma}(r)\Theta_m(\theta), \tag{2}$$

where $\epsilon_{m,\sigma}$ is the corresponding eigenvalue.

The second-quantized Hamiltonian is then

$$H_s = \sum_{m\sigma}\epsilon_{m,\sigma}a^\dagger_{m,\sigma}a_{m,\sigma} + \sum_m \Omega_m\left(a^\dagger_{m,\uparrow}a_{m,\downarrow} + a^\dagger_{m,\downarrow}a_{m,\uparrow}\right), \tag{3}$$

where

$$\Omega_m = \Omega\int rdr\phi_{m,\uparrow}(r)I(r)\phi_{m,\downarrow}(r). \tag{4}$$

As illustrated in Fig. 2, when the scalar Stark potential is sufficiently deep, the radial mode functions $\phi_{m,\sigma}$ for different angular-momentum modes m overlap with each other, and are all concentrated on a ring, with radius $r_0 = \sqrt{l\omega^2/2}$. The Hamiltonian can then be further simplified as

$$H_{\text{ring}} = \sum_{m\sigma}\xi_{m,\sigma}a^\dagger_{m,\sigma}a_{m,\sigma} + h\sum_m\left(a^\dagger_{m,\uparrow}a_{m,\downarrow} + a^\dagger_{m,\downarrow}a_{m,\uparrow}\right), \tag{5}$$

where $\xi_{m,\uparrow(\downarrow)} = \xi_m \pm (\alpha m + \frac{\delta}{2})$, $\xi_m = m^2\hbar^2/(2Mr_0^2)$, $\alpha = l\hbar^2/(Mr_0^2)$, and $h = \Omega I(r_0)$. Throughout the work, we will use $E_l = \alpha l$ as the unit of energy.

Hamiltonian (5) is easily diagonalized with $H_{\text{ring}} = \sum_{m,\beta=\pm}\lambda_{m,\beta}a^\dagger_{m,\beta}a_{m,\beta}$. Here $a_{m,\beta}$ are the annihilation operators of the SOAM coupled helicity bands, with $\lambda_{m,\pm} = \xi_m \mp \sqrt{h^2 + (\alpha m + \delta/2)^2}$. These expressions are the angular analog of those in the momentum space of a one-dimensional system under spin-orbit coupling.

We consider a contact s-wave interaction between the two spin species. The interaction term under the single-mode approximation is written as

$$H_{\text{int}} = V^{(1)}\sum_{mm'q}a^\dagger_{m',\uparrow}a^\dagger_{q-m',\downarrow}a_{q-m,\downarrow}a_{m,\uparrow}, \tag{6}$$

where we dropped the angular dependence of $V^{(1)}$ since $\phi_{m,\sigma}(r)$ almost overlap for different angular-momentum modes m. In writing down Eq. (6), we also assumed a weak-coupling scenario, where the interaction strength is weak enough such that radial modes other than $n = 1$ are not excited. We renormalize the bare interaction rate $V^{(1)}$ through [21,23]

$$\frac{1}{V^{(1)}} = \sum_m\frac{1}{E_B^{(1)} - \xi_{m,\uparrow} - \xi_{-m,\downarrow}}, \tag{7}$$

where $E_B^{(1)}$ is the energy of the two-body bound state in the same ring potential but without the SOAM coupling.

B. Hamiltonian for scenario II

Similarly, under the single-mode approximation, the Hamiltonian for scenario II is written as

$$H^{(2)} = \sum_{m\sigma}\xi_{m,\sigma}a^\dagger_{m,\sigma}a_{m,\sigma} + h\sum_m(a^\dagger_{m,\uparrow}a_{m,\downarrow} + a^\dagger_{m,\downarrow}a_{m,\uparrow}) + \sum_m\xi_m b^\dagger_m b_m + V^{(2)}\sum_{mm'q}a^\dagger_{m',\uparrow}b^\dagger_{q-m'}b_{q-m}a_{m,\uparrow}. \tag{8}$$

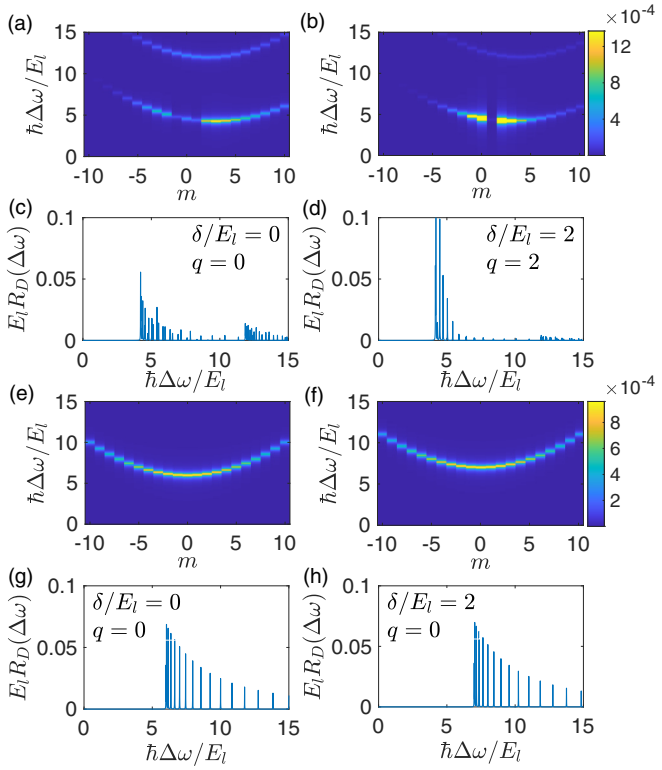

FIG. 4. (a)–(d) Direct Raman spectrum with SOAM coupling. (a) Angular-momentum-resolved spectrum $R_{\rm D}(m, \Delta\omega)$ for a molecular state with $q = 0$. (b) Angular-momentum-resolved spectrum for a molecular state with $q = 2$. (c) Integrated spectrum $R_{\rm D}(\Delta\omega)$ for the state in (a). (d) Integrated spectrum for the state in (b). (e)–(h) Direct Raman spectrum without SOAM coupling, under the same parameters as those in (a)–(d), respectively. Other parameters are $l = 5$, $E_B^{(1)}/E_l = -6$, and $\Omega/E_l = 0.18$.

Here we assumed that the two atoms have the same mass M and taken the two-photon detuning $\delta = 0$. The bare interaction rate $V^{(2)}$ is renormalized through

$$\frac{1}{V^{(2)}} = \sum_m \frac{1}{E_B^{(2)} - \xi_{m,\uparrow} - \xi_{-m}}, \tag{9}$$

where $E_B^{(2)}$ is the two-body bound-state energy under the same setup, but without the SOAM coupling.

III. MOLECULAR STATE FOR SCENARIO I

We are now in a position to solve for the molecular state. For the first scenario, the molecular state can be written as

$$\left|\Psi_q^{(1)}\right\rangle = \sum_m \sum_{\alpha,\beta=\pm} C_m^{\alpha\beta} a_{m,\alpha}^\dagger a_{q-m,\beta}^\dagger |0\rangle, \tag{10}$$

where $C_m^{\alpha\beta}$ is the wave function in the angular-momentum space, q is the orbital angular momentum, and $|0\rangle$ is the vacuum sate. From the Schrödinger's equation $(H_{\rm ring} + H_{\rm int})|\Psi_q^{(1)}\rangle = E_q^{(1)}|\Psi_q^{(1)}\rangle$, we derive the closed equation

$$\frac{2}{V^{(1)}} = \sum_m \left[\frac{(u_m v_{q-m} - v_m u_{q-m})^2}{E_q^{(1)} - \lambda_{m,+} - \lambda_{q-m,+}} + \frac{(u_m v_{q-m} - v_m u_{q-m})^2}{E_q^{(1)} - \lambda_{m,-} - \lambda_{q-m,-}} + \frac{(u_m u_{q-m} + v_m v_{q-m})^2}{E_q^{(1)} - \lambda_{m,+} - \lambda_{q-m,-}} + \frac{(u_m u_{q-m} + v_m v_{q-m})^2}{E_q^{(1)} - \lambda_{q-m,+} - \lambda_{m,-}} \right]. \tag{11}$$

Here the coefficients $\{u_m, v_m\}$ relate the spin and helicity basis and are given by

$$u_m = \sqrt{\frac{1}{2}\left[1 - \frac{\alpha m + \delta/2}{\sqrt{h^2 + (\alpha m + \delta/2)^2}}\right]}, \tag{12}$$

$$v_m = \sqrt{\frac{1}{2}\left[1 + \frac{\alpha m + \delta/2}{\sqrt{h^2 + (\alpha m + \delta/2)^2}}\right]}. \tag{13}$$

The molecular binding energy is then $E_M^{(1)} = E_q^{(1)} - E_{\rm th}$, where the threshold energy of the two-body scattering states is $E_{\rm th} = 2\min(\lambda_{m,+})$.

In Figs. 3(a) to 3(c), we show the calculated binding energy $E_M^{(1)}$ as a function of the angular momentum q, under different detunings. While the distribution is generally asymmetric with respect to $q = 0$ under a finite detuning [Figs. 3(b) and 3(c)], the ground state lies in a finite q sector under a sufficiently large detuning [Fig. 3(c)]. This picture is consistent with the vortex state in an SOAM coupled Fermi superfluid, which starts to emerge above a critical detuning. In Figs. 3(d) to 3(f), we further plot the angular-momentum distribution of ground-state wave functions, where the location of the dip in $|C_m^{++}|^2$ corresponds to one half the quantized orbital angular momentum of the molecule. The dip is directly related to the induced p-wave pairing symmetry under the SOAM coupling. More specifically, while only s-wave interactions exist between fermions with distinct spins, single-particle states dressed by SOAM couplings are superpositions of both spins, and therefore, can feature a p-wave pairing symmetry. This is manifested in the finite values of $C_m^{\alpha\alpha}$ ($\alpha = \pm$), which should obey the relation $C_m^{\alpha\alpha} = -C_{q-m}^{\alpha\alpha}$ according to the wave function Eq. (10). The wave function thus vanishes at $C_{q/2}^{\alpha\alpha}$, leading to the dip at $m = q/2$ in Fig. 3.

We propose to detect the molecular state through a direct Raman spectroscopy in which a two-photon Raman process couples the spin-down state to a third state $|3\rangle$ that is not interacting with either spin species. For a coupling term $H_{\rm R} = \Omega_{\rm R} \sum_m e^{i\Delta\omega t} a_{m,3}^\dagger e^{-il\theta} a_{m,\downarrow}$, the angular-momentum-resolved rate of transition is given by [29]

$$\begin{aligned} R_{\rm D}(m, \Delta\omega) &= -\sum_{m',\beta=\pm} {\rm Im} \frac{\left|\left\langle m', \beta\right| a_{m,\downarrow} \left|\Psi_q^{(1)}\right\rangle\right|^2}{\Delta\omega - \left(\lambda_{m',\beta} + \xi_{m-l} - E_q^{(1)}\right) + i0^+} \\ &= 4\pi \sum_{\beta=\pm} \left|C_m^{+\beta} v_m - C_m^{-\beta} u_m\right|^2 \\ &\quad \times \delta\left[\Delta\omega - \left(\lambda_{q-m,\beta} + \xi_{m-l} - E_q^{(1)}\right)\right]. \end{aligned} \tag{14}$$

Here $|m, \beta\rangle = a_{m,\beta}^\dagger |0\rangle$, $\Omega_{\rm R}$ is the amplitude of the coupling term, the factor $e^{-il\theta}$ comes from the gauge transformation,

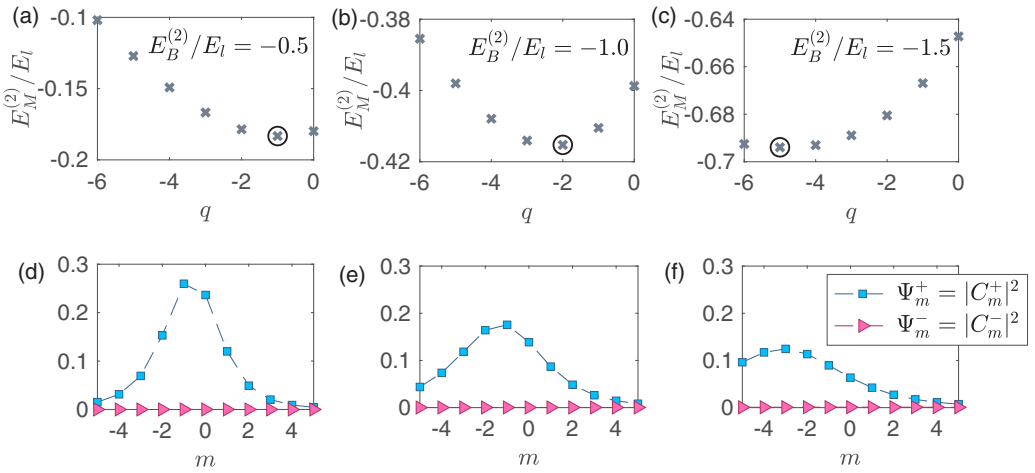

FIG. 5. (a)–(c) The molecular binding energy $E_M^{(2)}$ as functions of the angular momentum q, under interaction strengths (a) $E_B^{(2)}/E_l = -0.5$, (b) $E_B^{(2)}/E_l = -1.0$, (c) $E_B^{(2)}/E_l = -1.5$. (d–f) The ground-state molecular wave function in the discretized angular-momentum space (characterized by m), under the parameters in (a)–(c), respectively. For all calculations, we fix $l = 5$ and $\Omega/E_l = 0.2$.

and $\Delta\omega$ is the detuning of two-photon coupling under an appropriate rotating frame where $|\downarrow\rangle$ and $|3\rangle$ are degenerate in the absence of the SOAM coupling and interaction. The overall transition rate is $R_{\rm D}(\Delta\omega) = \sum_m R_{\rm D}(m, \Delta\omega)$.

The numerically evaluated spectra are shown in Figs. 4(a) to 4(d). The finite molecular angular momentum can be identified from the angular-momentum-resolved spectroscopy [Fig. 4(b)]. The discretized peaks in the integrated spectra [Figs. 4(c) and 4(d)] are a direct consequence of the quantized angular momentum. By contrast, in Figs. 4(e) to 4(h), we show the spectra under the same parameters, but without SOAM coupling. Particularly, the spectra in Figs. 4(e) and 4(f) are symmetric with respect to $m = 0$, indicating molecules with zero center-of-mass angular momentum. While the angular-momentum-resolved spectroscopy is helpful for identifying molecules with finite center-of-mass momentum, it is experimentally demanding. In comparison, the integrated spectra [Figs. 4(c) to 4(h)], which are much easier to access in experiments, are generally not sensitive to the angular momentum of molecules. Nevertheless, the following scenario II is designed such that both the angular-momentum-resolved and integrated spectra are accessible.

IV. MOLECULAR STATE FOR SCENARIO II

The molecular state of the second scenario can be written as

$$\left|\Psi_q^{(2)}\right\rangle = \sum_m \sum_{\beta=\pm} C_{m,\beta} a_{m,\beta}^\dagger b_{q-m}^\dagger |0\rangle, \tag{15}$$

where $C_{m,\beta}$ is the wave function and q represents the molecular angular momentum.

From the Schrödinger's equation $H^{(2)}|\Psi_q^{(2)}\rangle = E_q^{(2)}|\Psi_q^{(2)}\rangle$, the closed equation for the molecular energy is

$$\frac{1}{V^{(2)}} = \sum_m \left(\frac{u_m^2}{E_q^{(2)} - \xi_{m-q} - \lambda_{m,+}} + \frac{v_m^2}{E_q^{(2)} - \xi_{m-q} - \lambda_{m,-}} \right), \tag{16}$$

where u_m and v_m are the same as Eqs. (12) and (13). The molecular binding energy is $E_M^{(2)} = E_q^{(2)} - [\min(\xi_m) + \min(\lambda_{m,+})]$.

We show the molecular energies as functions of the orbital angular momentum in Figs. 5(a) to 5(c). The ground-state molecules all have a finite angular momentum due to the interplay of the SOAM coupling and spin-selective interaction. Their angular momenta are also reflected in the wave functions, which are asymmetric in the angular momentum space, as shown in Figs. 5(d) to 5(f).

As a convenient scheme to resolve the finite angular momentum, we propose to perform an inverse Raman spectroscopy [3] with Laguerre-Gaussian beams. The Raman process couples atomic population in a spectator $|3\rangle$, to an empty state $|b\rangle$, in the presence of the SOAM coupled atoms. The coupling Hamiltonian is written as

$$H_{\rm R} = \Omega_{\rm R} \int d\mathbf{r} e^{im\theta} \psi_b^\dagger(\mathbf{r}) \psi_3(\mathbf{r}), \tag{17}$$

where m indicates the angular-momentum transform of the Raman probe, which consists of two Laguerre-Gaussian beams with different orbital angular momentum. Assuming atoms in state $|3\rangle$ have zero angular momentum, the Raman probe thus picks out wave-function components $C_{q-m,\lambda}$ in the molecular wave function, enabling an angular-momentum-resolved spectroscopy. Note that this Raman process is different from the one in the direct Raman spectroscopy for scenario I, where there is zero net angular-momentum transfer.

The angular-momentum-resolved transfer rate of the inverse Raman spectroscopy is

$$\begin{aligned} R_{\rm I}(m, \Delta\omega) &= -\sum_{m',\beta=\pm} {\rm Im} \frac{\left|\left\langle \Psi_q^{(2)} | b_m^\dagger | m', \beta \right\rangle\right|^2}{\Delta\omega - \left(E_q^{(2)} - \lambda_{m',\beta}\right) + i0^+} \\ &= \pi \sum_{\beta=\pm} |C_{q-m,\beta}|^2 \delta\left[\Delta\omega + \left(\lambda_{q-m,\beta} - E_q^{(2)}\right)\right]. \end{aligned} \tag{18}$$

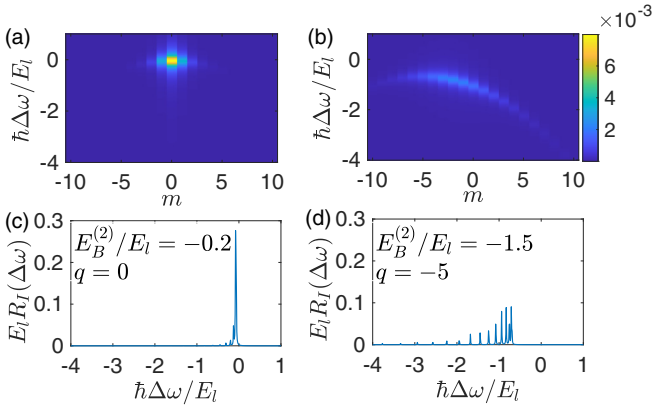

FIG. 6. (a) Inverse angular-momentum-resolved Raman spectrum for a molecular state with $q = 0$ and $E_B^{(2)}/E_l = -0.2$. (b) Inverse angular-momentum-resolved Raman spectrum for a molecular state with $q = -5$ and $E_B^{(2)}/E_l = -1.5$. (c,d) are the integrated inverse spectra $R_I(\Delta\omega) = \sum_m R_I(m, \Delta\omega)$ for (a,b), respectively. Other parameters are $l = 5$ and $\Omega/E_l = 0.2$.

Here $\Delta\omega$ is the two-photon detuning of the Raman probe, under the rotating frame where $|b\rangle$ and $|3\rangle$ are degenerate in the absence of the SOAM coupling and interaction.

As illustrated in Fig. 6(b), the asymmetry of the inverse Raman spectrum (with respect to $m = 0$) clearly reveals the finite angular momentum of the corresponding molecular state. Note that the angular-momentum resolution is achieved through the Laguerre-Gaussian beams used for the inverse Raman spectroscopy.

V. SUMMARY

We show that the unique pairing mechanism under the SOAM coupling is reflected in the molecular state under the corresponding configurations. Using two different scenarios as examples, we demonstrate the interplay of the SOAM coupling, Zeeman fields, and interaction can give rise to molecular states with finite angular momentum, which are the angular analogues of the spin-orbit-coupling-induced molecular states in Fermi gases [28,30,31]. We propose to detect the molecular angular momentum through direct and inverse Raman spectroscopy. Since molecular states persist at temperatures higher than the superfluid temperature, they are an ideal candidate for experimental detection, particularly in light of heating introduced by the SOAM coupling. Further, in contrast to the spin-orbit-coupling-induced finite center-of-mass momentum pairing states (either pairing superfluid or molecules) [7], the angular momentum of the molecular states under study here are quantized, and are therefore more accessible to experimental detection. Therefore, our work provides a practical route toward the confirmation of the unique pairing mechanism under synthetic gauge fields such as spin-orbit coupling and SOAM coupling.

ACKNOWLEDGMENTS

This work was supported by the National Natural Science Foundation of China (Grants No. 11974331, No. 12104406, and No. 11974384) and the National Key R&D Program (Grant No. 2017YFA0304100). K.-J.C. acknowledges support from the startup grant of Zhejiang Sci-Tech University (Grant No. 21062338-Y). S.-G.P. acknowledges support from the Natural Science Foundation of Hubei Province (Grant No. 2021CFA027).

APPENDIX: RENORMALIZATION RELATION

Here we derive in detail the renormalization relations Eqs. (7) and (9) in the main text. We only focus on the first scenario since the second scenario is similar.

We start by considering a two-dimensional Fermi gas under the same in-plane ring potential as in the main text, but without the SOAM coupling. The Hamiltonian is

$$\mathcal{H}^{(1)} = \sum_\sigma \int d\mathbf{r}\psi_\sigma^\dagger(\mathbf{r})K_\sigma(\mathbf{r})\psi_\sigma(\mathbf{r}) + +g^{(1)}\int d\mathbf{r}\psi_\uparrow^\dagger(\mathbf{r})\psi_\downarrow^\dagger(\mathbf{r})\psi_\downarrow(\mathbf{r})\psi_\uparrow(\mathbf{r}). \tag{A1}$$

Similar to the derivation leading to Eq. (3) where a tightly confined ring geometry is assumed, we have

$$\mathcal{H}^{(1)} = \sum_{m\sigma}\epsilon_{m,\sigma}a_{m,\sigma}^\dagger a_{m,\sigma} + \sum_{mm'q} V_{m,m',q}^{(1)} a_{m',\uparrow}^\dagger a_{q-m',\downarrow}^\dagger a_{q-m,\downarrow}a_{m,\uparrow}, \tag{A2}$$

where $V_{m,m',q}^{(1)} = \frac{g^{(1)}}{2\pi}\int r dr \phi_{m',\uparrow}(r)\phi_{q-m',\downarrow}(r)\phi_{q-m,\downarrow}(r)\phi_{m,\uparrow}(r)$.

Writing the two-body bound state as $|\Psi^{(1)}\rangle = \sum_m C_m a_{m,\uparrow}^\dagger a_{-m,\downarrow}^\dagger|0\rangle$, we have (from the Schrödinger's equation)

$$C_m = \frac{S_m^{(1)}}{E_B^{(1)} - \epsilon_{m,\uparrow} - \epsilon_{-m,\downarrow}}, \tag{A3}$$

$$S_m^{(1)} = \sum_{m'} V_{m',m,q=0}^{(1)} C_{m'}, \tag{A4}$$

where $E_B^{(1)}$ is the two-body bound-state energy in the absence of SOAM coupling. The idea is to use $E_B^{(1)}$ as a parameter to characterize the interaction strength. For weak trapping potentials, $E_B^{(1)}$ approaches $-\hbar^2/Ma_{2D}^2$ where a_{2D} is the s-wave scattering length in two dimensions. As the trapping strength increases, the relation between $E_B^{(1)}$ and a_{2D} can be derived explicitly by renormalizing $g^{(1)}$ through the free-space T-matrix, followed by calculating the two-body bound-state problem of Hamiltonian (A1). We leave this to future studies.

When the ring potential is sufficiently deep, $\phi_{m,\sigma} \simeq \phi_{m',\sigma}$, which leads to $V_{mm'q}^{(1)} \approx V^{(1)}$, meaning the interaction strength is independent of m and m'. The bound-state energy thus satisfies

$$\frac{1}{V^{(1)}} = \sum_m \frac{1}{E_B^{(1)} - \xi_{m,\uparrow} - \xi_{-m,\downarrow}}. \tag{A5}$$

This is the renormalization relation Eq. (7). As a final remark, we note that, although the summation in the renormalization relation above converges, it helps Eq. (11) to converge faster when applied.

[1] Y.-J. Lin, K. Jiménez-García, and I. B. Spielman, Nature (London) **471**, 83 (2011).

[2] P. Wang, Z.-Q. Yu, Z. Fu, J. Miao, L. Huang, S. Chai, H. Zhai, and J. Zhang, Phys. Rev. Lett. **109**, 095301 (2012).

[3] L. W. Cheuk, A. T. Sommer, Z. Hadzibabic, T. Yefsah, W. S. Bakr, and M. W. Zwierlein, Phys. Rev. Lett. **109**, 095302 (2012).

[4] V. Galitski and I. B. Spielman, Nature (London) **494**, 49 (2013).

[5] N. Goldman, G. Juzeliūnas, and P. Öhberg, and I. B. Spielman, Rep. Prog. Phys. **77**, 126401 (2014).

[6] H. Zhai, Rep. Prog. Phys. **78**, 026001 (2015).

[7] W. Yi, W. Zhang, and X. Cui, Sci. China Phys. Mech. Astron. **58**, 1 (2015).

[8] J. Zhang, H. Hu, X. J. Liu, and H. Pu, Annu. Rev. Cold At. Mol. **2**, 81 (2014).

[9] L. Zhang and X. J. Liu, in *Synthetic Spin-Orbit Coupling in Cold Atoms*, edited by W. Zhang, W. Yi, and C. A. R. Sá Melo, (World Scientific, Singapore, 2018), pp. 1–87.

[10] D. Zhang, T. Gao, P. Zou, L. Kong, R. Li, X. Shen, X.-L. Chen, S.-G. Peng, M. Zhan, H. Pu, and K. Jiang, Phys. Rev. Lett. **122**, 110402 (2019).

[11] H.-R. Chen, K.-Y. Lin, P.-K. Chen, N.-C. Chiu, J.-B. Wang, C.-A. Chen, P.-P. Huang, S.-K. Yip, Y. Kawaguchi, and Y.-J. Lin, Phys. Rev. Lett. **121**, 113204 (2018).

[12] Y.-X. Hu, C. Miniatura, and B. Grémaud, Phys. Rev. A **92**, 033615 (2015).

[13] M. DeMarco and H. Pu, Phys. Rev. A **91**, 033630 (2015).

[14] K. Sun, C. Qu, and C. Zhang, Phys. Rev. A **91**, 063627 (2015).

[15] C. Qu, K. Sun, and C. Zhang, Phys. Rev. A **91**, 053630 (2015).

[16] L. Chen, H. Pu, and Y. Zhang, Phys. Rev. A **93**, 013629 (2016).

[17] X.-L. Chen, S.-G. Peng, P. Zou, X.-J. Liu, and H. Hu, Phys. Rev. Res. **2**, 033152 (2020).

[18] K.-J. Chen, F. Wu, J. Hu, and L. He, Phys. Rev. A **102**, 013316 (2020).

[19] L. Chen, Y. Zhang, and H. Pu, Phys. Rev. Lett. **125**, 195303 (2020).

[20] Y. Duan, Y. M. Bidasyuk, and A. Surzhykov, Phys. Rev. A **102**, 063328 (2020).

[21] K.-J. Chen, F. Wu, S.-G. Peng, W. Yi, and L. He, Phys. Rev. Lett. **125**, 260407 (2020).

[22] L.-L. Wang, A.-C. Ji, Q. Sun, and J. Li, Phys. Rev. Lett. **126**, 193401 (2021).

[23] K.-J. Chen, F. Wu, L. He, and W. Yi, Phys. Rev. Res. **4**, 033023 (2022).

[24] X. Cui, B. Lian, T.-L. Ho, B. L. Lev, and H. Zhai, Phys. Rev. A **88**, 011601(R) (2013).

[25] R. A. Williams, M. C. Beeler, L. J. LeBlanc, K. Jimenez-Garcia, and I. B. Spielman, Phys. Rev. Lett. **111**, 095301 (2013).

[26] Z. Fu, L. Huang, Z. Meng, P. Wang, L. Zhang, S. Zhang, H. Zhai, P. Zhang, and J. Zhang, Nat. Phys. **10**, 110 (2014).

[27] F. Wu, G.-C. Guo, W. Zhang, and W. Yi, Phys. Rev. Lett. **110**, 110401 (2013).

[28] L. Zhou, X. Cui, and W. Yi, Phys. Rev. Lett. **112**, 195301 (2014).

[29] S.-G. Peng, X.-J. Liu, H. Hu, and K. Jiang, Phys. Rev. A **86**, 063610 (2012).

[30] L. Dong, L. Jiang, H. Hu, and H. Pu, Phys. Rev. A **87**, 043616 (2013).

[31] V. B. Shenoy, Phys. Rev. A **88**, 033609 (2013).